



The Role of Silicon in Silicon-Graphite Composite Electrodes Regarding Specific Capacity, Cycle Stability, and Expansion

Erfan Moyassari,^{1,z} Thomas Roth,¹ Simon Kücher,¹ Chia-Chin Chang,² Shang-Chieh Hou,³ Franz B. Spingler,¹ and Andreas Jossen^{1,4}

¹Chair for Electrical Energy Storage Technology (EES), TUM School of Engineering and Design, Technical University of Munich (TUM), Arcisstr. 21, 80333 Munich, Germany

²Department of Greenery, National University of Tainan, Tainan, 70101, Taiwan

³Department of Materials Science and Engineering, National Cheng Kung University, Tainan, 70101, Taiwan

⁴Munich School of Engineering (MSE), Technical University of Munich (TUM), Lichtenbergstr. 4a, 85748 Garching, Germany

One promising way of compensating for the repeated volume expansion and contraction of silicon as an anode active material in lithium ion batteries (LIBs) is to embed silicon within a graphite matrix. Silicon-graphite (SiG) composites combine the advantageous properties of graphite, i.e., large electrical conductivity and high structural stability, with the advantageous properties of silicon, i.e., high theoretical capacity. Graphite has a much lower volume expansion upon lithiation ($\approx 10\%$) than pure silicon ($\approx 300\%$) and provides a mechanically stable matrix. Herein, we present an investigation into the electrochemical performance and thickness change behavior of porous SiG anode compositions with silicon contents ranging from 0 wt% to 20 wt%. The electrode composites were studied using two methods: in situ dilatometry for the thickness change investigation and conventional coin cells for the assessment of electrochemical performance. The measurements show that the initial thickness change of SiG electrodes increased significantly with the silicon content, but it leveled off during cycling for all compositions. There appears to be a correlation between silicon content and capacity loss, but no clear correlation between thickness change and capacity loss rate was found.

© 2022 The Author(s). Published on behalf of The Electrochemical Society by IOP Publishing Limited. This is an open access article distributed under the terms of the Creative Commons Attribution 4.0 License (CC BY, <http://creativecommons.org/licenses/by/4.0/>), which permits unrestricted reuse of the work in any medium, provided the original work is properly cited. [DOI: 10.1149/1945-7111/ac4545]



Manuscript submitted November 5, 2021; revised manuscript received December 10, 2021. Published January 5, 2022.

Energy storage systems for electric vehicles call for high-energy battery cells, and weight, costs, and volume need to be optimized at the same time. Given that the efficiency of these properties are critical in an electric vehicle application, the energy per mass and per volume, i.e., the specific or volumetric energy, this area has become a focus of ongoing research in battery development.^{1,2} The specific and volumetric energies are dependent on cell voltage and capacity, so they increase at greater cell capacities, whereas most LIBs are limited in their voltage range.³ The cell capacity is determined by the electrode capacities of the anode and the cathode. The choice of anode active material shows potential for improvement in increasing the energy density of a battery cell.⁴ The ideal anode active material should offer long cycle life, low toxicity, low cost, and a high specific capacity. The state-of-the-art anode active material of commercial lithium-ion batteries is graphite.⁵ The reasons for using graphite include its low cost and high electrochemical reversibility. Nevertheless, the storage mechanism in graphite anodes, in which lithium ions reside between the graphite layers, limits the theoretical specific capacity to 372 mAh g⁻¹.⁶ One alternative to graphite is silicon. It is environmentally friendly, inexpensive, and is the second most common chemical element in the Earth's crust. It is well suited for alloying with lithium and provides a specific capacity of up to 3578 mAh g⁻¹, which is almost ten times higher than graphite. In addition, the volumetric capacity is as high as 2400 mAh cm⁻³. However, its high volume change is a major disadvantage when using pure silicon as an anode active material. The volume change is as high as $\approx 300\%$ between complete delithiation and lithiation, which is much higher than the $\approx 10\%$ volume change for graphite⁷ and can lead to "cracking" of the silicon electrodes. In this case, a degradation of the silicon in crystalline form and amorphization at the same time occurs in the electrode, mainly during the first lithiation.^{7,8} Moreover, the particles partially revert to a metastable crystalline phase at a deep lithiation (below 50 mV).⁹ Tranchot, et al.⁷ states that the morphology of the silicon composite does not change considerably from 2nd to 10th cycle. This could support the

fact that cracking and silicon particle fractures happen mainly during the first cycle. Upon repeated alloying and dealloying of lithium with silicon, a steady breaking and rebounding of the silicon-silicon bonds is observed, leading to mechanical stress and silicon particle cracking.¹⁰ The direct consequences of the particle cracking include capacity loss, an increase in internal resistance, lower coulombic efficiency, and SEI instability.^{6,7} In addition to the SEI layer reforming at cracked silicon surfaces, the high volume changes also make it difficult for the SEI to achieve a stable state. The SEI (in the expanded state, "lithiation"), can break up when the Si particles contract again. This process exposes a new silicon surface, and the SEI reforms. As a result, the SEI becomes thicker and thicker during the following cycles⁹ and further increases the capacity loss of silicon electrodes. Wu and Cui⁹ exhibited a 70% decrease in capacity in the first five cycles of a pure silicon electrode. Accordingly, one frequent research question addresses how to minimize the detrimental properties of silicon. Chae, et al.¹¹ presented approaches to make silicon more suitable as an anode material. The latter include reducing the silicon particle size to nano-size and cladding the surface, both of which reduce the volume change. Ko, et al.¹² have also focused on reducing particle volume change by means of nano-sizing. Moreover, methods such as thin films with honeycomb patterns as electrodes, porous structures, or graphite composite materials such as silicon graphite have been presented and their advantages discussed. The idea in combining silicon and graphite materials is to combine the respective advantages and to mitigate the disadvantages. SiG as an anode material for LIBs has been the subject of numerous research studies. In these studies, the percentage of silicon in combination with graphite varies. Otero, et al.⁴ investigated SiG as an anode active material with a silicon content ranging from 0 wt% to 100 wt%. Furthermore, the volumetric capacity increases greatly in a silicon content range of up to about 25 wt%. At higher levels of silicon content, the volumetric capacity still increases, but at lower rates. Therefore, significant advantages are achieved only up to a silicon content of 40 wt%. The specific capacity, on the other hand, seems to increase linearly with the silicon content. In addition, a half cell with 25 wt% silicon was compared to a cell with 100 wt% graphite and a cell with

^zE-mail: erfan.moyassari@tum.de

100 wt% silicon as anode material with respect to specific capacity. Wetjen, et al.¹³ investigated LIB full cells with LiFePO₄ as the cathode and SiG alloy as anode material with a silicon content ranging from 20 wt% to 60 wt%. They showed that, with increasing silicon content, the delithiation capacity increases, but a greater capacity loss over the number of cycles occurs at the same time. Moreover, the coulombic efficiency over the entire number of cycles was highest for the least silicon content of 20 wt%. Especially in cycles 10 to 40, the coulombic efficiency was found to be decisively lower at high silicon contents. In addition, both the irreversible capacity loss due to cycling and the relative volume of the SEI was larger for at higher levels of silicon content.

The focus of this work is investigating the thickness change of various SiG compositions using a dilatometer. Dilatometric measurements have been widely utilized since the late 1970s for recording the dilation of the host compounds caused by the intercalation of guest ions or molecules inserted into the host layers.¹⁴ Biberacher, et al.¹⁵ developed an electrochemical dilatometer and were able to show the volume change linked to the lithium-ion intercalation and deintercalation into the graphitic host material. Winter, et al.¹⁴ measured the layered samples, such as highly oriented pyrolytic graphite (HOPG), as a host material. The HOPG was cycled at a high scan rate of 10 mV s⁻¹ between 3.0 V and 0.5 V vs Li/Li⁺ in an ethylene carbonate (EC) and dimethyl carbonate (DMC) based electrolyte, which led to a thickness change of 10%. Ohzuku, et al.¹⁶ reported the volume change data of graphite with lithium perchlorate (LiClO₄) in EC/DMC solvents as an electrolyte during the first charging of the electrochemical cell. They showed that the graphite expanded more than 10%, which they attributed to the expansion at the initial part of the primary reduction. Sauerteig, et al.¹⁷ investigated the reversible and irreversible thickness change of a graphite/NMC cell. Their results indicate that the porosity strongly influences the irreversible thickness change of the electrodes, whereas the influence of the porosity on the reversible thickness change is negligible. Nagayama, et al.¹⁸ reported a dilatometric method for characterizing lithium insertion electrodes. The area-specific deformation (ASD) was determined to be the crucial parameter in characterizing lithium insertion electrodes. The LiNi_{1/3}Co_{1/3}Mn_{1/3}O₂ electrode was stable (0 μm mAh⁻¹ cm⁻²) up to a voltage of 4.15 V vs an LTO electrode. At a potential greater than 4.15 V, the ASD was determined to be about 1 μm mAh⁻¹ cm⁻². In,¹⁹ Rieger, et al. performed a dilatometric study on the thickness change of a commercial graphite/lithium-cobalt dioxide (LCO) pouch cell. The graphite electrode expanded by 5.2%, whereas the thickness change of LCO electrode was 1.8%. In our recent work²⁰ we reported the thickness changes of various electrodes during cycling and compared them to crystal structure changes measured by XRD from the scientific literature. Moreover, the reliability and the electrochemical performance of the dilatometry setup were thoroughly validated.

In our earlier study,²¹ the focus was on the first (de-)lithiation performance of the SiG electrode composites at a varying silicon content using electrochemical analyses and neutron depth profiling (NDP). In the present work, we extend these investigations to a higher number of cycles than those investigated in²¹ while focusing on both the electrochemical performance and the thickness change behavior of the same electrode composites of SiG electrodes at a silicon content ranging from 0 wt% to 20 wt%.

Experimental

Electrode preparation.—The electrode samples were prepared to have various silicon/graphite ratios as active materials. The amount of active material was 95 wt% in all of the electrode compositions. For this purpose, the active material content of silicon having the same compositions discussed in²² and graphite (MG13AN, China Steel Chemical Co.) varied at a silicon/graphite ratio of 0/95 (SiG00), 3/92 (SiG03), 5/90 (SiG05), 7/88 (SiG07), 10/85 (SiG10), 15/80 (SiG15), and 20/75 (SiG20), respectively. Other

5 wt% non-active materials included 2 wt% SuperP (MMM Carbon, Belgium), 2.50 wt% carboxymethyl cellulose (CMC, Sigma-Aldrich Co., Germany), and 0.50 wt% styrene butadiene rubber (SBR, Zeon Co., Japan). The slurry preparation and mixing procedure of the electrode samples as well as the schematic presentation of the electrode sample compositions were mentioned in our earlier study.²¹ The initial coating thicknesses of the electrodes were 31 μm, 34 μm, 40 μm, 36 μm, 39 μm, 44 μm, and 29 μm for SiG00, SiG03, SiG05, SiG07, SiG10, SiG15, and SiG20, respectively.

Silicon preparation.—Commercial silicon powder (99.9%, Fuzhou Hokin Chemical Technology, China) at a micrometric particle size was used as a starting material with no further purifying procedure. The silicon powder was placed in a stainless 500 ml vial along with stainless balls at a dimension of 3 mm. The ball-to-powder mass ratio was 20:1. The vials were sealed under an argon atmosphere in a glove box. The milling procedure type was horizontal edge milling machine (HEMM) performed at room temperature for 9 h using a planetary miller (PM 400, Retsch, Germany) at a rotation speed of 300 RPM. The milled silicon was introduced into a PP (polypropylene) jar along with ZrO₂ balls at a dimension of 2 mm and an ethanol medium. The ball-to-powder mass ratio was 20:1. The wet milling was performed at room temperature using a rotation mixer at 250 RPM. After wet milling, the powder was filtered and dried at 120 °C in a vacuum for 12 h. The resulting milled powder was used to manufacture the aforementioned electrodes.

Coin cells.—The coin cells were built under an argon atmosphere (O₂, H₂O < 0.1 ppm) inside a glovebox (MBraun Inertgas-System GmbH, Germany). Two coin cells were built from every SiG composition. The results of all coin cells pairs were in good agreement, so only the results from one cell per composite will be presented hereinafter. The coin cells (Hohsen Corp., Japan) were composed of a single-side-coated SiG ($\phi \approx 14$ mm) as a working electrode, Li metal foil with $\phi \approx 15.6$ mm (Rockwood Lithium, USA) as a counter electrode, and two glass fiber separators (VWR, USA). Each separator had a diameter of 16 mm and a thickness of about 260 μm; 100 μl of electrolyte were used. Since it is of great importance for the SiG electrodes to have a stable solid electrolyte interface (SEI) layer to ensure a longer lifetime, 1 M LiPF₆ with EC:EMC (1:1 wt:wt) and an additional 10 wt% FEC were used (from Solvionic, France). The electrochemical cells were assembled using two spacer disks, 1 × 1.0 mm plus 1 × 0.5 mm, a spring, then sealed with a fitting ring, as shown in Fig. 1b.

After assembly, the cells were rested for 6 h and then operated for 8 cycles using a constant current lithiation and delithiation protocol (including the formation cycles). All the cells discussed herein were cycled at a current density of 75 μA cm⁻². The cells delivered different capacities, based on the varying silicon content, so the C rates varied between ≈ 0.033 C and ≈ 0.1 C. These measurements were performed inside a temperature controlled climate chamber (Vötsch Industrietechnik GmbH, Germany) at 25 °C using a battery cycler (CTS, Basytec GmbH, Germany).

Dilatometer.—An ECD-3-Nano electrochemical dilatometer from EL-Cell GmbH was used for the dilatometry measurements. The latter device enables measurement of the thickness change of individual electrodes during cycling. A schematic of the dilatometry setup is shown in Fig. 1a. The electrodes were separated by a T-frit, which is a porous borosilicate glass separator that mechanically decoupled the working electrode from the counter electrode. This approach prevents measurement errors of the working electrode thickness that may be caused by volume changes of the counter electrode. The thickness change of the working electrode was recorded by a capacitive displacement sensor (Linear Variable Differential Transformer, LVDT) via a spacer disk and a stainless steel membrane.²³ The sensor resolution was < 5 nm. This

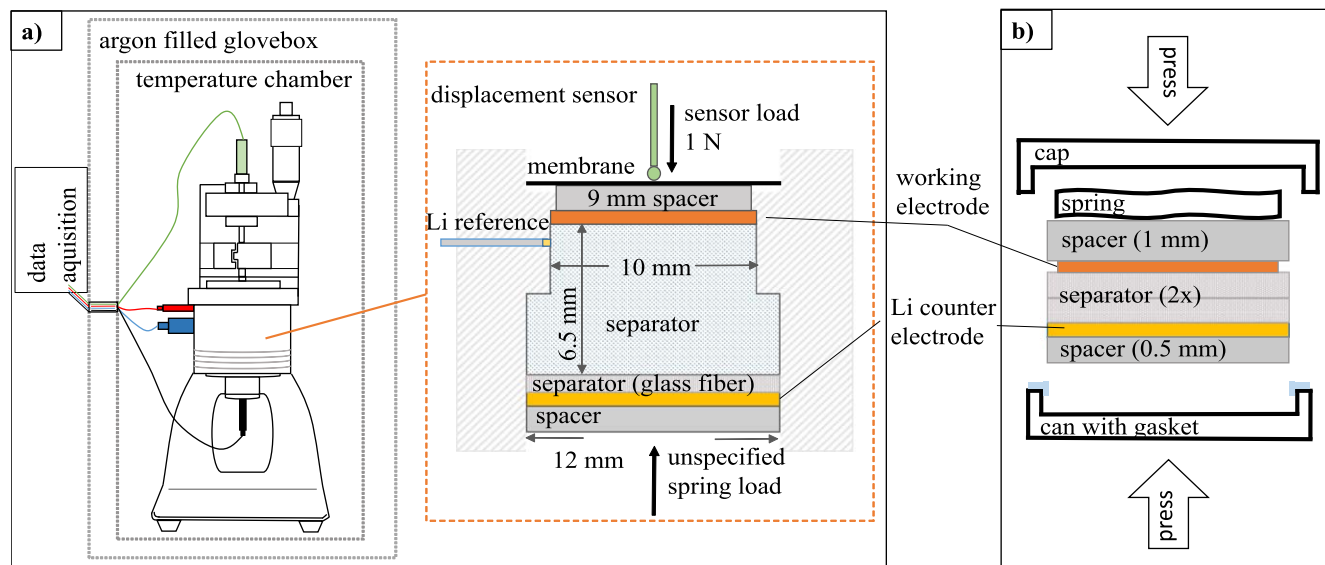


Figure 1. Schematic representation of (a) ECD-3-Nano dilatometer placed in a climate chamber inside the glovebox and (b) the coin cell setup used in this study.

corresponds to approximately 0.005% of the initial thickness of the electrodes under investigation. The displacement sensor was pressed onto the surface of the electrode at a force of 1 N. This ensured continuous contact between the sensor and the surface. According to the manufacturer, the drift of the dilatometer is less than 20 nm h^{-1} . The 12 mm diameter counter electrode is made of metallic lithium.²⁴ The working electrode diameter was 10 mm. The dilatometer was assembled and operated under an argon atmosphere inside a glovebox ($\text{O}_2, \text{H}_2\text{O} < 0.1 \text{ ppm}$). The ambient temperature during operation of the dilatometer was $35 \text{ }^\circ\text{C}$. This approach improves cycling performance in comparison to operation at $25 \text{ }^\circ\text{C}$, as discussed in our earlier report.²⁰ Similar to the coin cells, 1 M LiPF_6 with EC:EMC (1:1 wt:wt) and 10 wt% FEC as an additional additive were used as the electrolyte for the electrochemical cell in the dilatometer. The electrochemical cell was filled with approximately 1 ml of electrolyte. A VMP3 potentiostat (Bio-Logic, France) was used for the test protocol. The thickness of the sample tested was recorded every five seconds. Similar to the coin cell experiments, the current density in all dilatometry experiments was $75 \mu\text{A cm}^{-2}$. The resulting C rates in the dilatometry measurements varied because the capacities of the electrodes differed.

Results and Discussion

We will first discuss the electrochemical analyses based on coin cells, which will be followed by the results from the dilatometry measurements. The validation of the dilatometry setup used in this paper has been thoroughly discussed in, Ref. 20 so it will not be repeated here.

Electrochemical analysis of coin cells.—Figures 2a–2g shows the potential vs specific capacities of each electrode from the coin cell measurements for the eight cycles. A specific color was adapted for each cycle number, from 1 to 8, which remained constant among the various SiGs. The potential curves were plotted for both lithiation, which is shown in solid lines, and delithiation, which is shown in dashed lines having the same color as that of the lithiation curve. Furthermore, the active material composition (in wt%) of the electrodes is described using the numbers in combination with SiG as the active material composite, e.g., SiG00 and SiG20 demonstrated 0 wt% and 20 wt% of silicon in combination with 95 wt% and 75 wt% of graphite, respectively. As shown in Figs. 2a–2g, the specific capacity of the electrodes as well as the capacity loss per cycle increased at an elevating silicon content in the electrodes. For example, the specific capacity of delithiation for the 8 cycles is listed in Table 1 for various SiGs in $\text{mAh g}_{\text{AM}}^{-1}$.

The same trend applied to the hysteresis between the lithiation and delithiation potential curves. In the literature, the value of voltage hysteresis of graphite (10 to 30 mV) is described as being significantly lower than that of silicon (250 to 320 mV).²⁵ These values make sense if one considers that more capacity loss processes occur with silicon than with graphite, as mentioned earlier.⁹ Consequently, a higher silicon content in SiG composite will lead to a larger voltage difference, and more hysteresis will occur. This hysteresis due to polarization can be explained by the continuous SEI formation. The SEI layer forms during the lithiation procedure and is due to the electrolyte decomposition at the electrode surface at lower potentials.²⁶ The formation and growth of SEI as an electron insulator layer used for Li^+ conduction should stop after several cycles.²⁷ However, in the case of continuous SEI formation, the polarization of the electrode increased.⁶ This effect was more dominant at higher levels of silicon content. Moreover, each electrode composition experienced a higher capacity loss at the first cycle, which equalized itself to some extent during the following cycles. As mentioned in, Ref. 21 this phenomenon can be attributed to an irreversible capacity from some modifier, like pitch. Pitch is usually used as precursor for achieving a carbon-coated surface in active materials used to enhance cycling performance. It is assumed to lead to more irreversible capacity from SEI formation upon the first cycle of lithiation.

In addition, Wetjen, et al.¹³ demonstrated a strong potential course change around a delithiation potential of $\approx 0.25\text{--}0.5 \text{ V}$ vs Li/Li^+ for various SiG electrode compositions (with 20–60 wt% silicon content) when moving towards higher cycle numbers, which is stated to be the transition from the crystalline silicon phase of $\text{Li}_{15}\text{Si}_4$ to the amorphous silicon phase. Furthermore, it is also stated that the silicon is the main reason behind the capacity loss at delithiation potentials higher than 0.25 V at higher cycle numbers. However, in the present study, the measurement data did not show a strong change in the potential course of the SiG electrode composites (see Figs. 2a–2g), which may indicate that no silicon phase transition from crystalline to amorphous was observed. This can be explained in two different ways; First, in the present work, various SiG electrode compositions containing less silicon content were investigated and, second, this study focuses on a total number of 8 cycles. Nevertheless, the capacity loss in the present work also increased at a higher silicon content.

The specific capacity difference between the lithiation and delithiation cycles can be best compared via coulombic efficiency (CE). In Fig. 3a, the CE of the coin cell measurements are plotted for different SiGs in different cycles. The initial cycle had a significantly lower CE, which is typical of silicon-based electrodes.²⁸ The measurement data showed that the CE stabilized after the initial

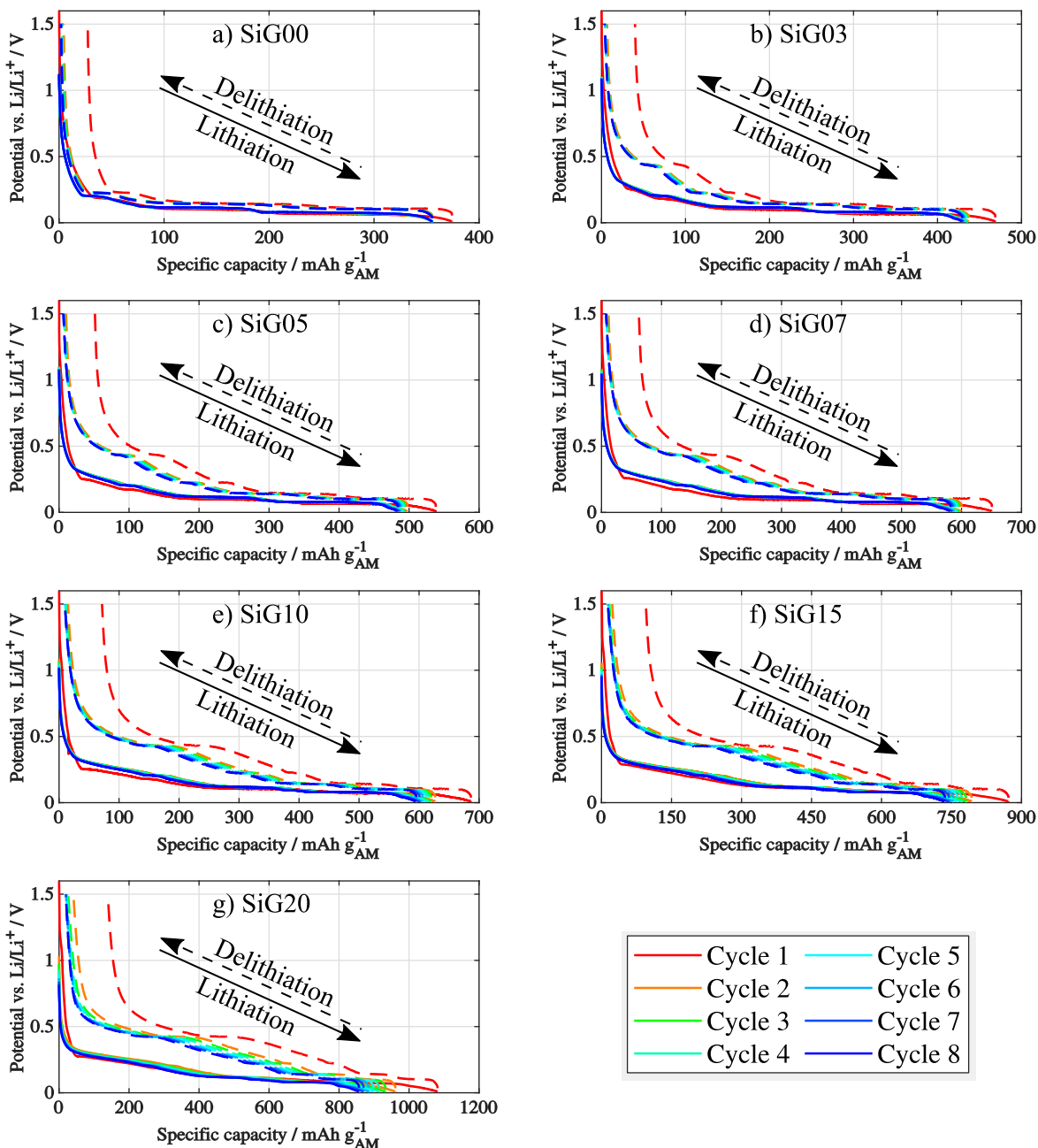


Figure 2. Potential vs specific capacity with 10 mV as lithiation cutoff criteria for first eight cycles for (a) SiG00, (b) SiG03, (c) SiG05, (d) SiG07, (e) SiG10, (f) SiG15, and (g) SiG20.

cycles. Nevertheless, higher levels of silicon content led to lower CE levels even after stabilization. For example, the CE of the third cycle was 99.5%, 98.9%, 98.4%, 98.5%, 98.2%, 97.9%, and 97.2% for SiG00, SiG03, SiG05, SiG07, SiG10, SiG15, and SiG20, respectively.

Figure 3b shows the evolution of the specific capacity for each composite and that for different cycles, in solid lines. The theoretical specific capacity of the same SiG composite calculated using data from the literature⁶ is shown in dashed lines having the same color. The theoretical specific capacity of the SiGs was determined according to Eq. 1,

$$C_{\text{SiG, theoretical}} = w_G \cdot C_G + w_{\text{Si}} \cdot C_{\text{Si}} \quad [1]$$

where c is the theoretical capacity and w is the mass fraction of graphite and silicon, respectively. Increasing the silicon content led to a higher difference between the measured and theoretical

capacities of a SiG composition and increased the negative slope of the capacity loss. For SiG03 and SiG20 by way of example, the difference between the capacities of the 1st and 8th cycle from the theoretical capacity of the corresponding SiG varied between 39.28–42.88 mAh g_{AM}⁻¹ and 70.9–175.3 mAh g_{AM}⁻¹, respectively. This might be explained by the silicon-dependent loss processes discussed above.⁹ Furthermore, in order to show the linearity of capacity loss as a function of silicon content, the sum of the capacity loss during the 8 cycles is shown in Fig. 3c with respect to different silicon contents. As discussed earlier in this study, the existence of pitch as an additive in the electrode coating preparation process caused a higher capacity drop, as can be seen in the first two cycles of SiG00. This may have been the reason for the negative part of the black line (cycle #1–8) in Fig. 3c. The aforementioned observations apply to the results from both our methods—the previously discussed conventional coin cell and the dilatometry measurements which are discussed in the following section.

Table I. Specific capacity of delithiation, in mAh g_{AM}⁻¹, and the coulombic efficiency (CE), in percentage, for the coin cell measurements of different SiGs with cutoff voltage of 10 mV.

	1 st cycle	2 nd cycle	3 rd cycle	4 th cycle	5 th cycle	6 th cycle	7 th cycle	8 th cycle	Average value
SiG00	346.86	351	352.01	352.57	352.88	353.13	353.25	353.42	351.89
CE	92.71	98.75	99.09	99.25	99.33	99.41	99.44	99.50	—
SiG03	428.9	430.5	430.7	430.2	429.54	428.1	426.55	425.3	428.72
CE	91.5	98.54	98.85	98.94	99.02	99.05	99.08	99.11	—
SiG05	486.9	487.3	486.5	485.4	483.85	482	479.8	477.5	483.66
CE	90.49	97.99	98.42	98.54	98.6	98.65	98.7	98.72	—
SiG07	588.2	588.3	586.8	584.9	583.1	580.5	577.3	573.9	582.88
CE	90.42	98.08	98.49	98.6	98.65	98.67	98.68	98.69	—
SiG10	614.8	611.9	608.8	605	600.9	596	591	585.8	601.78
CE	89.57	97.62	98.18	98.28	98.33	98.37	98.39	98.42	—
SiG15	777.1	770.1	764.4	757.1	748.4	739.6	730.8	722.4	751.24
CE	89.12	97.11	97.86	98.07	98.11	98.13	98.15	98.18	—
SiG20	942.3	920.2	906.9	892.6	878.2	864.5	851.2	837.9	886.73
CE	87.12	95.73	97.18	97.55	97.71	97.76	97.77	97.75	—

Dilatometry measurements.—This section will present and discuss the dilatometry measurement results for various SiG electrode compositions. In order to distinguish the thickness change of the electrodes during formation cycles from that of cycles in which the SEI layer was already stable, the dilatometry results were separated into two parts; I) formation cycles (first 2–3 cycles) and II) post-formation cycles (from the fourth cycle onwards). Based on the measurement protocol, the dilatometry cells mostly cycled for six full cycles.

Formation cycles during which the SEI layer forms and stabilizes.—Figures 4a–4g shows the results of operando dilatometry for various SiG electrode compositions during the formation cycles. Each subplot, from a to g, presents the results of a different SiG composite, as mentioned on the subplot itself. The left and right y-axes represent the potential (in V) and thickness change (in percentage) vs the specific capacity of the dilatometry cell, respectively. The lithiation potential curves are black solid-lines, the delithiation potential curves are gray dashed-lines, the lithiation thickness change is depicted as dark blue solid-lines, and the delithiation thickness change appears as light blue dashed-lines. The cycle numbers are indicated next to the thickness change curves using hashtags. In addition, the end of the (de-)lithiation curves are the same both for potential and thickness change curves. The same presentation was used for the following Figs. 5a–5g in the post-formation cycles.

The relative thickness change of the electrodes increased in parallel with an increasing silicon content. As an example, the lithiation thickness change in the second cycle for SiG00, SiG03, SiG05, SiG07, SiG10, SiG15, and SiG20 were 5.36%, 9.33%, 11.95%, 17.28%, 18.04%, 26.81%, and 32.43%, respectively. The same trend of a higher specific capacity at a higher silicon content was observable during the formation cycles. For instance, the specific capacity at the second cycle for different SiGs, from SiG00 to SiG20, was 362.55, 492.33, 507.12, 628.71, 719.89, 822.71, and 925.62 mAh g_{AM}⁻¹, respectively.

Comparing the resulting specific capacity of the SiG electrode composites measured using dilatometry from Fig. 4 to those in Fig. 2 from coin cells showed a good level of plausibility for the electrochemical cell in dilatometry measurement setup. The small deviation between the (de-)lithiation of the coin cell and the electrochemical cell from the dilatometry can be explained by the larger overpotentials/polarization in the dilatometry cell, as was discussed in our previous study.²⁰ This deviation can be attributed to a different amount of electrolyte used in these measurements, or the difference in pressure buildup while assembling the electrochemical cells.

Post-formation cycles in which the SEI is assumed to be more stable.—During the post-formation cycles, the relative thickness change of the electrodes remained mostly constant; see Figs. 5a–5g. The average thickness change in the post-formation cycles was 5.30%, 6.51%, 9.04%, 12.46%, 14.79%, 20.99%, and 19.60% for SiG00, SiG03, SiG05, SiG07, SiG10, SiG15, and SiG20, respectively. Nonetheless, there were capacity losses for every SiG composition in the range of 0.23 mAh g_{AM}⁻¹ for SiG00 up to 31.26 mAh g_{AM}⁻¹ for SiG20. These losses were higher for electrodes having higher levels of silicon content. This might be explained by SEI reformation on freshly exposed active material surface due to the volume expansion of silicon. Consequently, the cell would have experienced an impedance increase and, through accumulation of the isolated SEI products, undesirable side reactions and polarization effects would then occur, thus affecting cell stability and electrochemical performance negatively.⁶ This is also supported by Dobrowolny, et al.,²⁹ who claimed that the significant structural change of the electrically insulating SEI layer, as well as the aforementioned consequences of the volume change, impair the cycling behavior and accelerate the aging of the electrochemical cell.

In agreement with prior dilatometry measurements for graphite anodes,¹⁹ there was a slope change for the thickness change due to the formation of LiC₁₂ in lithiation and delithiation directions, followed by a plateau. This kink can be seen at approximately 100 mAh g_{AM}⁻¹ for SiG00 in Fig. 5a. At higher levels of silicon content, the kink and the plateau moved to regions having higher specific capacities, e.g., 300 to 350 mAh g_{AM}⁻¹ for SiG07, and 500 to 550 mAh g_{AM}⁻¹ for SiG20. However, the location of the kink was always approximately 250 mAh g_{AM}⁻¹ below the maximum specific capacity of each cycle for all SiG composites. Given that this kink is characteristic of the lithiation of graphite, and it always occurred at the same location (shown in Fig. 6a), we concluded that the graphite was predominantly lithiated after the silicon and delithiated predominantly before the silicon. It has been shown in³⁰ and³¹ that, depending on the C rate, either silicon or graphite is lithiated first. At the C rates of 0.1 C and below used in the present study, the silicon was lithiated before the graphite. This could explain the location of the kink and plateau at a constant value below the maximum specific capacity. Simultaneously, the kink location could be dependent on the electrode potential, where the kink during the lithiation is located at around 0.1 V and during the delithiation at around 0.2 V for all SiGs. The electrode potentials at the kink location is exemplary shown for lithiation and delithiation in the Fig. 6b for the 4th cycle of different SiGs. Qualitatively, there was also a shift of the characteristic potential plateaus related to the graphite phase transition stages towards higher specific capacities with increasing silicon contents. The effect of the silicon content on

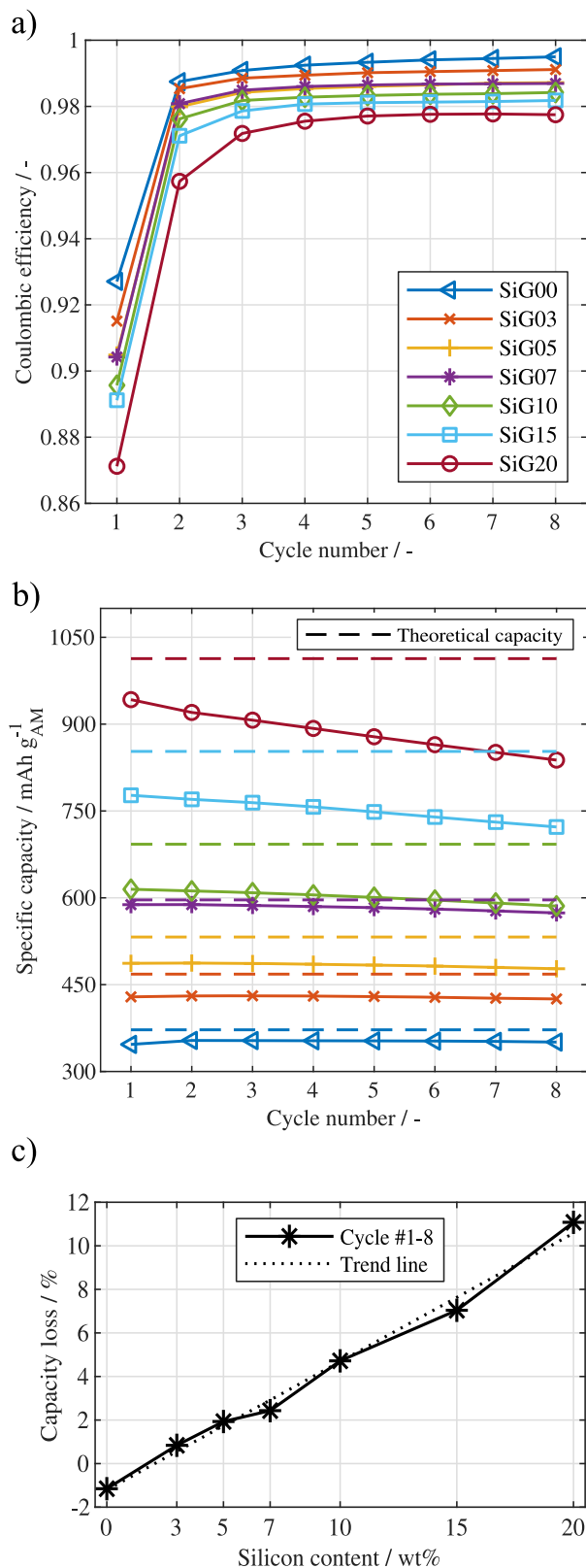


Figure 3. (a) Capacity loss calculated from coin cell measurements for different cycles and SiG composites, (b) delithiation capacity from coin cell measurements vs theoretical capacity calculated based on literature values and (c) overall relative capacity loss shown in respect to silicon content of the electrode composites.

the thickness change of the SiG electrodes is shown in Fig. 6c. Each line belongs to a different cycle, “o” to 1st cycle, “□” to mid-cycle ($\approx 3^{\text{rd}}$ cycle) and “x” to last cycle ($\approx 7^{\text{th}}$ cycle) of each electrode composition, respectively.

For SiG00 (i.e., pure graphite), the thickness change was almost constant from cycle to cycle. A higher silicon content led to a higher thickness change. Additionally, the higher the silicon content, the higher the difference between the first cycle thickness change and the post-formation cycles thickness change.

In order to better visualize the irreversible electrode expansion, Fig. 6d shows the cumulative irreversible thickness change of each SiG electrode during cycling, which is generally highest at the 1st cycle and increases with higher silicon contents. The curves of SiG07 and SiG10 almost overlap, and SiG15 has a lower irreversible thickness change than SiG07/SiG10. These results may indicate that the irreversible thickness change does not solely depend on the silicon content but also on other electrode properties, i.e. porosity and initial thickness. However, the fact that SiG15 exhibits a specific capacity below the trend (Fig. 6a), a larger polarization (Fig. 6b) and a higher than average capacity loss per cycle (Fig. 7f) points to SiG15 being an outlier.

Figures 7a–7g compares the relative thickness change for lithiation and delithiation to the capacity loss during delithiation for each cycle. The relative thickness change during lithiation corresponds to electrode expansion and, during delithiation, to electrode contraction, which are both expressed herein as positive values. The decreasing specific capacity loss per cycle was an indicator that the SiG electrode composites were still stabilizing. The capacity loss per cycle remained constant for SiGs up to 10 wt%, but it was still decreasing for SiG15 and SiG20. However, the capacity loss per cycle was significantly higher for SiGs than for the pure graphite anode.

The theoretical thickness change based on the volume change of each corresponding SiG electrode composite is shown in Fig. 7 for two extreme cases: A purely one-dimensional volume change (denoted as 1D), as well as a purely spherical volume change (denoted as 3D). In these theoretical cases, the SiG electrode composite was considered to be homogeneous, having volume-averaged properties of silicon and graphite particles, which is a simplification of the more complex volume change characteristics of silicon on the atomic-scale in.³² The 1D case assumed no volume change in the lateral electrode directions, with the electrode thickness change then equaling the theoretical volume change of the respective SiG composite. The one-dimensional thickness change Δt_{1D} was then calculated as shown in Eq. 2,

$$\Delta t_{1D} = \varphi_G \Delta \Delta V_G + \varphi_{Si} \Delta V_{Si} \quad [2]$$

where φ is the volume fraction, and ΔV is the maximum theoretical volume change of graphite and silicon, respectively. The volume fraction φ was calculated using the densities and mass fractions of the materials. The 3D case postulated uniform spherical volume change, with no preference in the expansion direction. As seen in Eq. 3, the spherical thickness change Δt_{3D} from the initial state was calculated based on the initial volume $V_0 = 100\%$ as well as the maximum spherical volumes of graphite and silicon. The binder and the other additives were neglected in both simplified calculations:

$$\Delta t_{3D} = \frac{\sqrt[3]{\frac{6}{\pi} \cdot (V_0 + \varphi_G \cdot \Delta V_G + \varphi_{Si} \cdot \Delta V_{Si})}}{\sqrt[3]{\frac{6}{\pi} V_0}} \quad [3]$$

In general, the relative thickness change during lithiation was higher than that of delithiation, especially in the formation cycles. The measured relative thickness change decreased for both lithiation and

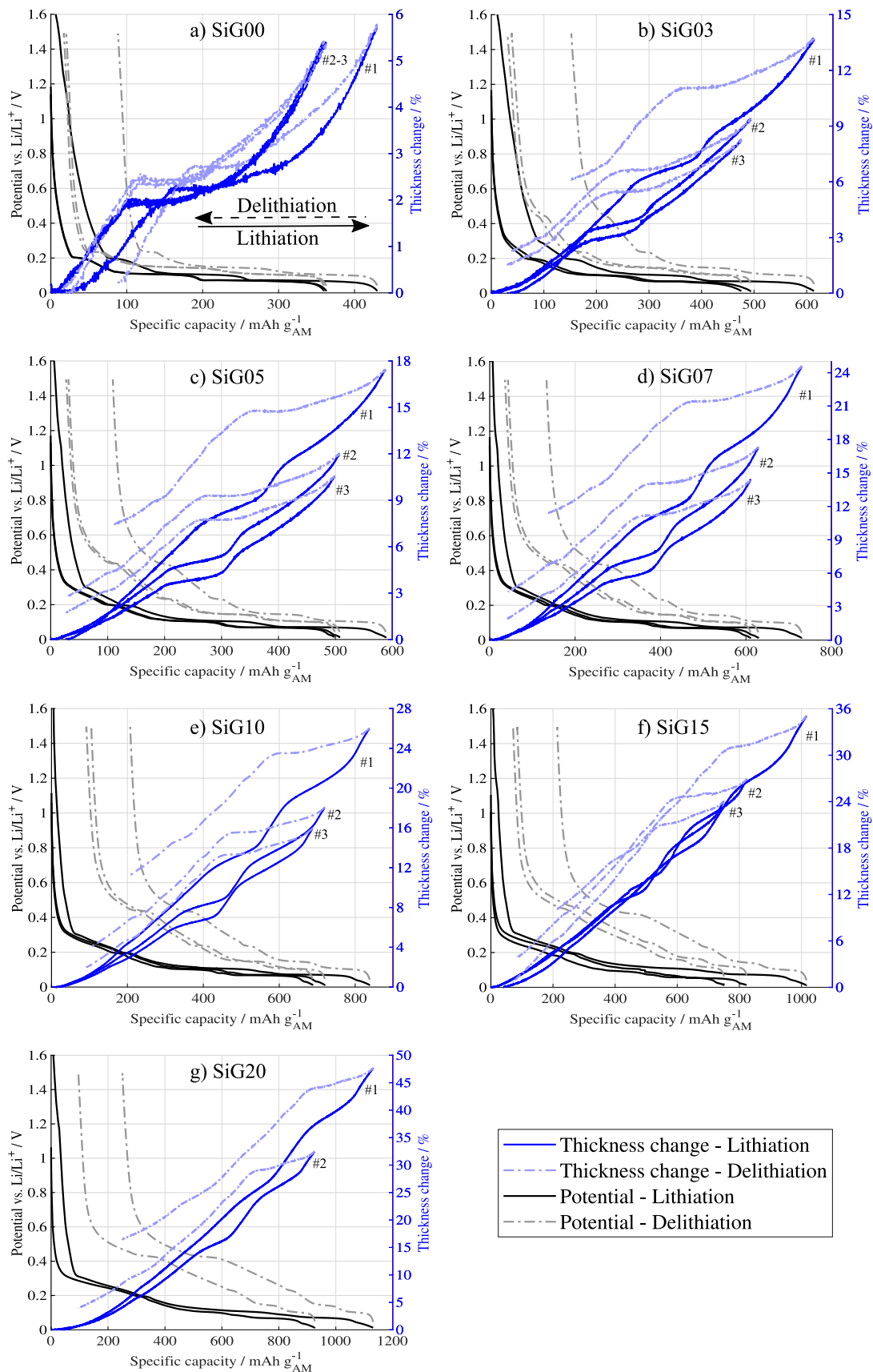


Figure 4. Results of dilatometry measurements of formation cycles shown for: (a) SiG00, (b) SiG03, (c) SiG05, (d) SiG07, (e) SiG10, (f) SiG15 and (g) SiG20. The arrows placed at lower right of the subplot (a) describe the direction of lithiation and delithiation.

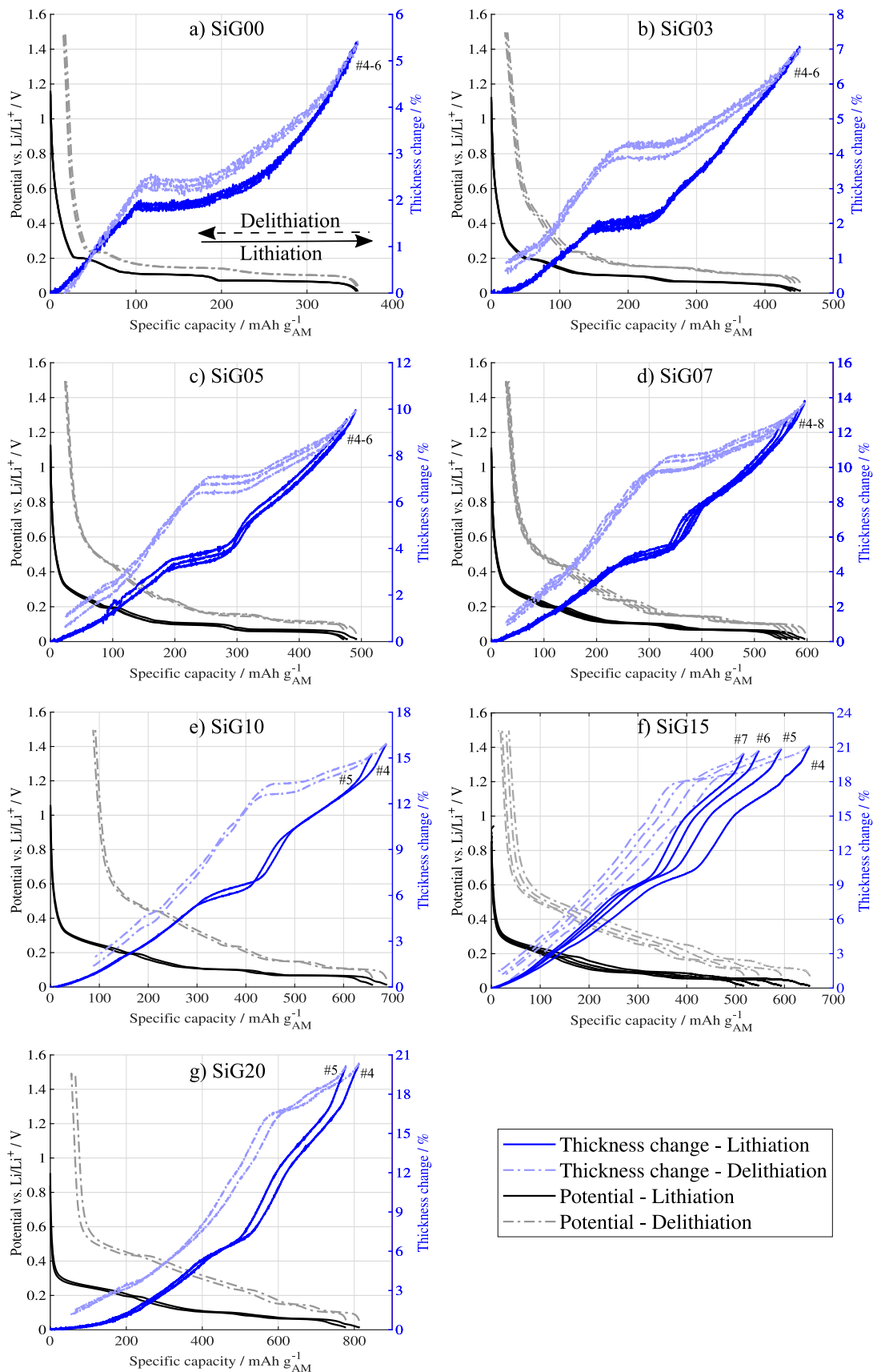


Figure 5. Results of dilatometry measurements of post-formation cycles shown for: (a) SiG00, (b) SiG03, (c) SiG05, (d) SiG07, (e) SiG10, (f) SiG15, and (g) SiG20. The arrows placed at lower right of the subplot (a) describe the direction of lithiation and delithiation.

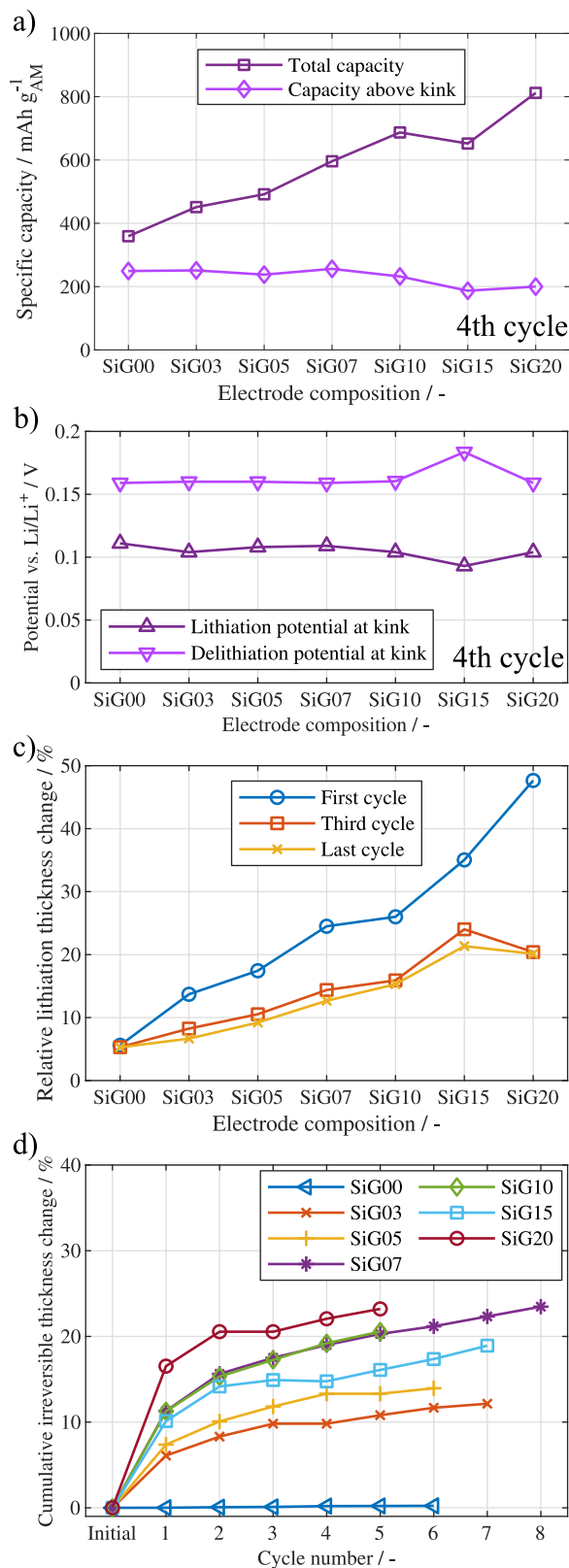


Figure 6. (a) Total specific capacity and specific capacity above kink at 4th cycle for different SiGs, (b) electrode potential at kink location at 4th cycle for different SiGs, (c) relative lithiation thickness change for different SiGs of first, middle and final cycles, (d) cumulative electrode thickness change for different SiGs at each cycle.

delithiation, and it stabilized slightly above the theoretical value for spherical volume change. This might indicate an anisotropic volume change on the electrode level, showing a preference in thickness direction in the formation cycles, whereas the volume change shifted to a more isotropic behavior during the post-formation cycles. On an electrode level, the anisotropic volume change might be explained by the limited lateral expansion due to the adjacent electrode active material and the constraining effect of the current collector foil. In contrast to the expansion, the contraction seemed to be generally lower and exhibited a lower slope. The contraction was thus closer to the isotropic volume change. During cycling, both the relative expansion and the relative contraction decreased, and a shift from anisotropic to isotropic volume change was observed. The exact reason for this behavior is still not fully understood. In case the electrode active material is considered to be a homogenous matrix, this might be caused by elastoplastic deformation during expansion, whereas the contraction is purely elastic. When particle behavior of silicon is considered, particle cracking might also be responsible for the difference in volume change between expansion and contraction that appeared to increase electrode volume irreversibly. It was already reported that particle cracking might lead to less well packed active material, thus steadily increasing the volume of the electrode.³³ It was also shown that particle cracking primarily occurs during the lithiation of silicon,³⁴ which might explain the higher volume change in the SiG composites during lithiation. Further focusing on the silicon particle properties, anisotropic swelling has also been reported.³⁵ It has been shown that silicon volume change is not ideally spherical, but elliptical or dumbbell-shaped.^{32,35} However, in a silicon graphite composite there would need to be a preference in orientation and silicon particle positioning; otherwise, an impact of particle volume change on electrode volume change could not be explained. Based on the SEM images given in our earlier study,²¹ there was no evident preference in the orientation of the silicon particles on the graphite structure.

The capacity loss per cycle was almost constant between cycles for silicon content levels from 3 wt% to 7 wt%, but it decreased slightly for silicon content levels above 10 wt%. Consequently, the high silicon content SiG composites were not yet stabilized after approximately 6 cycles. Notably, there was no apparent correlation between the relative thickness change and the capacity loss per cycle. Specifically, the stabilization of the relative thickness change during the post-formation cycles appeared to have no effect on capacity loss. Therefore, the shift from anisotropic to isotropic volume change may not have been responsible for the capacity loss of SiG electrode composites, and the capacity losses must be attributed mostly to silicon particle cracking and the instability of SEI.²⁸

It is worth mentioning that the electrode composites investigated in this work were non-calendered and highly porous samples. Based on calculations and data from the electrode manufacturer, the electrodes should have a porosity range of $\approx 60\%$ – 72% .²¹ Consequently, there may have been enough space within the structure of the electrodes to accommodate the volume change of the particles. The fact that our SiG00 had a relative thickness change of around 5.5%, which is lower than the values found in the literature for calendered graphite electrodes, supports this idea.^{17,19} This raises the question of how porosity and electrode thickness change, depending on each other.

Conclusions

The thickness change of SiG electrode composites at varying silicon content levels between 0 wt% and 20 wt% were measured by means of electrochemically stable in situ dilatometry. The electrodes were also investigated electrochemically via conventional coin cells. The comparable electrochemical behavior of the electrodes in the

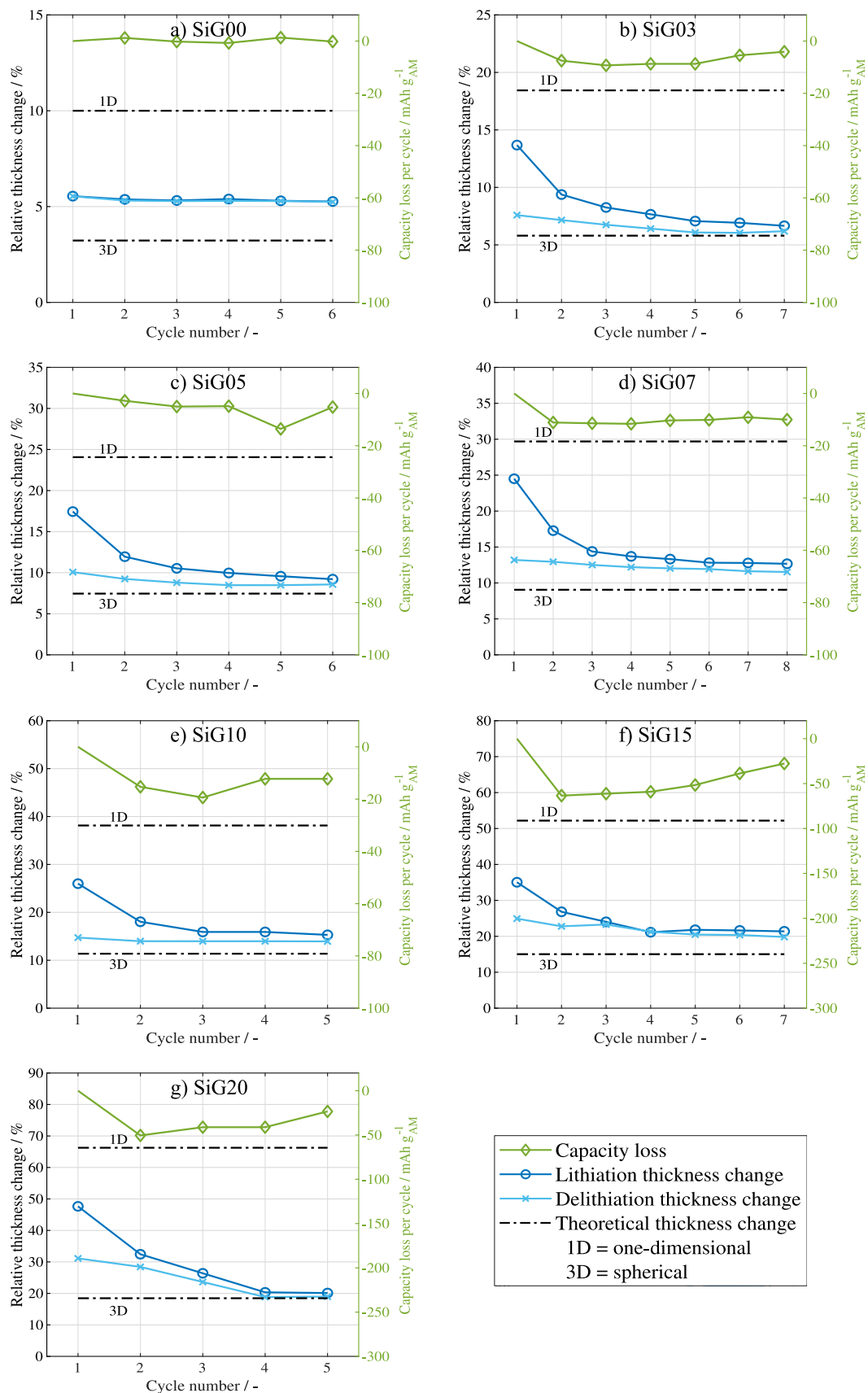


Figure 7. Capacity loss per cycle and comparison of relative thickness change for lithiation and delithiation cycles during dilatometry measurements shown for: (a) SiG00, (b) SiG03, (c) SiG05, (d) SiG07, (e) SiG10, (f) SiG15, and (g) SiG20. Calculated theoretical thickness change based on a purely one-dimensional (1D) as well as a purely spherical volume change (3D) is shown for each SiG composite.

experiments is proof of the plausibility of the dilatometry results. Increasing the silicon content led to higher specific capacities of the SiG electrodes. The relative capacity loss and the thickness change increased linearly with the silicon content as well. Based on the characteristic thickness change for the SiGs, we concluded that silicon predominantly lithiated before graphite, and delithiated after graphite. Generally, the thickness change was higher in the initial cycles, and then leveled off. This behavior was more pronounced at higher silicon content levels. Nevertheless, all of the samples eventually reached a steady, reversible thickness change per cycle. To explain this behavior, we have discussed hypotheses based on the preferential orientation and expansion of particles as well as their embedding in a stabilizing electrode matrix.

There appears to be no significant correlation between the leveling off of the relative thickness change and the capacity loss per cycle. We have argued that it is not the macroscopic structural changes of the electrode matrix which determine the capacity evolution, but rather the repeated microscopic expansion, cracking, and SEI formation on the particle-level.

Only non-calendered electrodes samples were investigated in this work. This leads to some uncertainty regarding the transferability of the results to practical, calendered electrodes. The interplay of electrode thickness and porosity changes as a result of particle-level volume changes and the initial porosity will be investigated in future work.

Acknowledgments

This work is financially supported by the German Federal Ministry of Education and Research (BMBF) in the project HighSafe II (03XP0306B) and by the Technical University of Munich (TUM). The responsibility for this publication lies with the authors.

ORCID

Erfan Moyassari  <https://orcid.org/0000-0002-3037-202X>

Thomas Roth  <https://orcid.org/0000000155432992>

Simon Kücher  <https://orcid.org/0000000322307356>

Franz B. Spingler  <https://orcid.org/0000-0002-6523-3986>

Andreas Jossen  <https://orcid.org/0000-0003-0964-1405>

References

- J. B. Goodenough and Y. Kim, "Challenges for rechargeable batteries." *J. Power Sources*, **196**, 6688 (2011).
- R. Schmich, R. Wagner, G. Hörpel, T. Placke, and M. Winter, "Performance and cost of materials for lithium-based rechargeable automotive batteries." *Nat. Energy*, **3**, 267 (2018).
- M. Winter, B. Barnett, and K. Xu, "Before Li Ion batteries." *Chem. Rev.*, **118**, 11433 (2018).
- M. Otero, C. Heim, E. P. M. Leiva, N. Wagner, and A. Friedrich, "Design-considerations regarding silicon/graphite and tin/graphite composite electrodes for lithium-ion batteries." *Sci. Rep.*, **8**, 1 (2018).
- B. Fuchsichler, C. Stangl, H. Kren, F. Uhlig, and S. Koller, "High capacity graphite silicon composite anode material for lithium-ion batteries." *J. Power Sources*, **196**, 2889 (2011).
- D. Ma, Z. Cao, and A. Hu, "Si-based anode materials for li-ion batteries: A mini review." *Nano-Micro Letter*, **6**, 347 (2014).
- A. Tranchot, A. Etienne, P. X. Thivel, H. Idrissi, and L. Roue, "In-situ acoustic emission study of Si-based electrodes for Li-ion batteries." *J. Power Sources*, **2**, 259 (2015).
- R. E. Ruther, K. A. Hays, S. J. An, J. Li, D. L. Wood, and J. Nanda, "Chemical evolution in silicon-graphite composite anodes investigated by vibrational spectroscopy." *ACS Appl. Mater. Interfaces*, **10**, 18641 (2018).
- H. Wu and Y. Cui, "Designing nanostructured Si anodes for high energy." *Nano Today*, **7**, 414 (2012).
- M. Wetjen, S. Solchenbach, D. Pritzl, J. Hou, V. Tileli, and H. A. Gasteiger, "Morphological changes of silicon nanoparticles and the influence of cutoff potentials in silicon-graphite electrodes." *J. Electrochem. Soc.*, **165**, 1503 (2018).
- S. Chae, M. Ko, K. Kim, K. Ahn, and J. Cho, "Confronting issues of the practical implementation of Si anode in high-energy lithium-ion batteries." *Joule*, **1**, 47 (2017).
- M. Ko, S. Chae, and J. Cho, "Challenges in accommodating volume change of si anodes for Li-Ion batteries." *ChemElectroChem*, **2**, 1645 (2015).
- M. Wetjen, D. Pritzl, R. Jung, S. Solchenbach, R. Ghadimi, and H. A. Gasteiger, "Differentiating the degradation phenomena in silicon-graphite electrodes for lithium-ion batteries." *J. Electrochem. Soc.*, **164**, A2840 (2017).
- M. Winter, G. H. Wrodnigg, J. O. Besenhard, W. Biberacher, and P. Novak, "Dilatometric investigations of graphite electrodes in nonaqueous lithium battery electrolytes." *J. Electrochem. Soc.*, **147**, 2427 (2000).
- W. Biberacher, A. Lerf, J. O. Besenhard, H. Möhwald, and T. Butz, "A high resolution dilatometer for in situ studies of the electrointercalation of layered materials." *Mater. Res. Bull.*, **17**, 1385 (1982).
- T. Ohzuku, N. Matoba, and K. Sawai, "Direct evidence on anomalous expansion of graphite-negative electrodes on first charge by dilatometry." *J. Power Sources*, **97-98**, 73 (2001).
- D. Sauersteig, S. Ivanov, H. Reinshagen, and A. Bund, "Reversible and irreversible dilation of lithium-ion battery electrodes investigated by in situ dilatometry." *J. Power Sources*, **342**, 939 (2017).
- M. Nagayama, K. Ariyoshi, Y. Yamamoto, and T. Ohzuku, "Characterization of lithium insertion electrodes by precision dilatometer: area-specific deformation of single electrode." *J. Electrochem. Soc.*, **161**, 1388 (2014).
- B. Rieger, S. Schlueter, S. V. Erhard, J. Schmalz, G. Reinhart, and A. Jossen, "Multi-scale investigation of thickness changes in a commercial pouch type lithium-ion battery." *Journal of Energy Storage*, **6**, 213 (2016).
- F. B. Spingler, S. Kücher, R. Phillips, E. Moyassari, and A. Jossen, "Electrochemically stable In Situ dilatometry of NMC, NCA and graphite electrodes for lithium-ion cells compared to XRD measurements." *J. Electrochem. Soc.*, **168**, 040515 (2021).
- E. Moyassari, L. Streck, N. Paul, M. Trunk, R. Neagu, C. C. Chang, S. C. Hou, B. Märkisch, R. Gilles, and A. Jossen, "Impact of silicon content within silicon-graphite anodes on performance and Li concentration profiles of Li-Ion cells using neutron depth profiling." *J. Electrochem. Soc.*, **168**, 020519 (2021).
- S. C. Hou, Y. F. Su, C. C. Chang, C. W. Hu, T. Y. Chen, S. M. Yang, and J. L. Huang, "The synergistic effects of combining the high energy mechanical milling and wet milling on Si negative electrode materials for lithium ion battery." *J. Power Sources*, **349**, 111 (2017).
- M. Hahn, H. Buqa, P. W. Ruch, D. Goers, M. E. Spahr, J. Ufheil, P. Novak, and R. Kötz, "A dilatometric study of lithium intercalation into powder-type graphite electrodes." *Electrochem. Solid-State Lett.*, **11**, 151 (2008).
- E. C. GmbH, Electrochemical dilatometer ECD-3-nano (2016), https://el-cell.com/wp-content/uploads/downloads/manuals/Manual_Dilatometer_ECD-3-nano_Release_1.34.pdf, 2017.
- V. A. Sethuraman, V. Srinivasan, A. F. Bower, and P. R. Guduru, "In Situ measurements of stress-potential coupling in lithiated silicon." *J. Electrochem. Soc.*, **157**, 1253 (2010).
- H. Wu et al., "Stable cycling of double-walled silicon nanotube battery anodes through solid-electrolyte interphase control." *Nat. Nanotechnol.*, **7**, 310 (2012).
- P. Verma, P. Maire, and P. Novak, "A review of the features and analyses of the solid electrolyte interphase in Li-ion batteries." *Electrochim. Acta*, **55**, 6332 (2010).
- Y. Jin, B. Zhu, Z. Lu, N. Liu, and Z. Jia, "Challenges and recent progress in the development of Si anodes for lithium-ion battery." *Adv. Energy Mater.*, **7**, 1700715 (2017).
- S. Dobrowolny, *Untersuchung von innovativen Silicium-Kohlenstoff-Komposit-Anoden für Lithium-Ionen-Batterien* (2017).
- K. Richter, T. Waldmann, N. Paul, N. Jobst, G. Scurtu, M. Hofmann, R. Gilles, and M. Wohlfahrt-Mehrens, "Low-temperature charging and aging mechanisms of Si/C composite anodes in Li-Ion batteries: an operando neutron scattering study." *ChemSusChem*, **13**, 529 (2020).
- K. P. C. Yao, J. S. Okasinski, K. Kalaga, J. D. Almer, and D. P. Abraham, "Operando quantification of (De)lithiation behavior of silicon-graphite blended electrodes for lithium-ion batteries." *Adv. Energy Mater.*, **9**, 1803380 (2019).
- M. T. McDowell, S. W. Lee, W. D. Nix, and Y. Cui, "Understanding the lithiation of silicon and other alloying anodes for lithium-ion batteries." *Adv. Mater.*, **25**, 4966 (2013).
- L. Y. Beaulieu, T. D. Hatchard, A. Bonakdarpour, M. D. Fleischauer, and J. R. Dahn, "Reaction of Li with alloy thin films studied by In Situ AFM." *J. Electrochem. Soc.*, **150**, A1457 (2003).
- H. B. Chew, B. Hou, X. Wang, and S. Xia, "Cracking mechanisms in lithiated silicon thin film electrodes." *Int. J. Solids Struct.*, **51**, 4176 (2014).
- X. H. Liu et al., "Anisotropic swelling and fracture of silicon nanowires during." *Nano Lett.*, **11**, 3312 (2011).